Available online at www.sciencedirect.com
ScienceDirect
International Journal of Heat and Mass Transfer 51 (2008) 3179–3189
International Journal of HEAT and MASS TRANSFER
www.elsevier.com/locate/ijhmt

Heat transfer in a rectangular chamber with differentially heated horizontal walls: Effects of a vibrating sidewall

Yiqiang Lin, Bakhtier Farouk *

Department of Mechanical Engineering and Mechanics, Drexel University Philadelphia, PA 19104, United States

Received 18 April 2007; received in revised form 4 August 2007
Available online 1 October 2007

Abstract

Heat transfer in a gas-filled closed enclosure with differentially heated horizontal walls is investigated numerically. One of the sidewalls vibrates with specified frequency and amplitude to induce forced convective flows in the enclosure. The vibrating and the stationary sidewalls are considered to be thermally insulated while the two horizontal walls are differentially heated. To simulate the flow field, the full compressible form of the Navier–Stokes equations is considered and solved by a highly accurate flux-corrected transport algorithm. In the numerical model, temperature dependant heat conductivity and viscosity are taken into account. The presence of acoustic streaming is found to have significant effect on the heat transfer. Also the presence of temperature gradients in the enclosure is found to affect the formation of acoustically induced streaming flows.

Keywords: Standing wave; Acoustic streaming; Heat transfer

1. Introduction

Heat transfer in differentially heated enclosures has been studied extensively in the past both experimentally and computationally. However, the effects of acoustically driven oscillatory flow fields on the convective heat transfer processes have been primarily studied experimentally. A detailed understanding of thermal energy transport in these problems is challenging. Sound sources whose elements move essentially sinusoidally may generate a flow field in which the particle velocities are not simply sinusoidal but a pattern of steady vortices (*streaming*) is often found in the body of the irradiated fluid. Sound at high intensity levels in gases and liquids, is accompanied by these second-order steady flow patterns.

Acoustic streaming is often observed where a standing wave is formed in a resonator driven by vibrating surface. With suitable design, this steady vortex flow can be employed for cooling of electronic systems in micro-gravity environment where free convective flows in fluids are greatly reduced or completely eliminated. Such flows can also aid mixing processes in containers and augment heat and mass transfer from resonator walls. Acoustically enhanced convection can be significant in zero- or micro-gravity environments where conduction is the only heat transfer mode.

While various analytical models are available for describing acoustic streaming phenomena, they are usually based on substantial approximations and the solutions are often limited to idealized conditions. The study of acoustic streaming started with the theoretical work of Lord Rayleigh [1]. He considered vortex flows occurring in a long pipe (Kundt's tube) as a result of the presence of a longitudinal standing wave. Westervelt [2] obtained a general vorticity equation and developed a general procedure for evaluating the streaming velocity induced by acoustical disturbances. Nyborg [3] reviewed the theories for calculating steady streaming associated with sound fields. An approximate solution was also developed by Nyborg [4] for sonically-induced steady flow near a fluid–solid interface

* Corresponding author.
E-mail address: bfarouk@coe.drexel.edu (B. Farouk).

0017-9310/$ - see front matter © 2007 Published by Elsevier Ltd.
doi:10.1016/j.ijheatmasstransfer.2007.08.005

Nomenclature

c	acoustic speed
c_v	specific heat
E	total energy
f	frequency
H	width of the enclosure
h	heat transfer coefficient
k	thermal conductivity
L	length of the enclosure
Nu	Nusselt number
p	pressure
q	heat flux
R	specific gas constant
t	time
T	temperature
u	velocity in the horizontal direction
v	velocity in the vertical direction
x	horizontal coordinate
y	vertical coordinate

Greek symbols

α	thermal diffusivity
γ	ratio of specific heats
μ	dynamic viscosity
ν	kinematic viscosity
ρ	density
τ	shear stress
ω	angular frequency

Subscripts

0	initial
B	bottom
T	left
st	streaming

subjected to the condition of known irrotational oscillatory velocity distribution in the vicinity of the interface. The effect of compressibility on acoustic streaming near a rigid boundary was investigated by Qi [5] with a theoretical study. Qi extended this study [5] to investigate acoustic streaming in a circular tube [6]. Vainshtein [7] combined the problems of Rayleigh streaming and Couette flow and investigated the effect of streaming on shear flows. Hamilton et al. [8] derived an analytic solution for the average mass transport velocity generated by a standing wave between parallel plates in different channel widths. Then the analysis method is extended to a gas in which heat conduction and dependence of viscosity on temperature are taken into account [9].

Richardson [10] analytically studied the effect of sound on natural convection from a horizontal cylinder subjected to transverse relative to the fluid in which it is immersed. Later, Richardson [11] presented shadowgraphs for a heated horizontal circular cylinder, subjected to transverse horizontal and vertical sound field. The shadowgraph demonstrated that the changes in local boundary layer thickness and heat transfer coefficient. Engelbrecht and Pretorius [12] experimentally studied the influence of sound waves on the transition from laminar to turbulent flow in the boundary layer associated with natural convective from a vertical flat plate with uniform heat flux. Gopinath and Mills [13,14] estimated the convective heat transfer from an isolated sphere in a standing sound field due to acoustic streaming in large streaming Reynolds numbers. Vainshtein et al. [15] performed the theoretical analysis on the heat transfer between two horizontal parallel plates in presence of a steady sonic wave propagated in the longitudinal direction. Mozurkewich [16] placed a heated cylindrical wire at a standing wave and measured the rate of heat transfer from the wire to the acoustic medium. *Nu* number showed a distinctive variation with acoustic amplitude. The similar experiments were reported by Gopinath and Harder [17] and Mozurkewich [18].

Yano [19] used an upwind TVD scheme to solve the full Navier–Stokes equation to investigate the turbulent acoustic streaming in a resonator. Aktas and Farouk [20] directly solved the compressible Navier–Stokes equations by the LCPFCT scheme. They classified the acoustic streaming to the classical streaming and irregular streaming. Acoustic streaming has received relatively less attention as a heat transfer enhancement mechanism. The mean flow motion due to streaming not only contributes to the convective heat transfer but also promotes the transition to turbulence [21]. Kawahashi and Arakawa [22] numerically studied acoustic streaming induced by finite-amplitude oscillation in a closed duct driven by a piston. The results showed velocity distributions in the oscillatory boundary layer and the change of the streaming profile due to the increase in the amplitude of oscillation, and the existence of a double layer in the vicinity of the duct wall. Kawahashi et al. [23] performed the experimental studies on the interaction of acoustic streaming with natural convection in a closed rectangular duct, and observed intensified steady streaming. Loh et al. [24,25] investigated the acoustic streaming induced by ultrasonic vibrations in an open space and the associated convection enhancement by theoretical, numerical and experimental methods.

Wan and co-workers [26–29] numerically and experimentally studied the fluid flow and heat transfer due to acoustic streaming in the gap between two horizontal beams, with the lower beam vibrating. The visualization

clearly showed that the vertical streaming can be induced by bimorph vibration, which enhanced heat transfer between the heated surface and surrounding air. In their numerical model, the governing equations are developed and solved for a three-layer structure, two thin boundary layers near the beams and one core region. The heat transfer coefficient is found to be strongly dependent on the width of channel, and a jump is revealed when bifurcation occurs.

Cheng and Hung [30] numerically investigated the effect of wall vibration on natural convection in a square enclosure. The integral form of conservation equations were solved by the two-stage pressure-correction method. In their model, the frequency of wall vibration is varied from 1 to 50 Hz. An unsteady flow recirculation was formed and enhanced heat transfer is reported. However, they did not report the formation of steady acoustic streaming. They also reported that the gravity condition has no marked effect on heat transfer. Kalabin and co-workers [31] numerically studied the periodic natural convection in an inclined square enclosure, where one side is maintained at a constant temperature and the temperature of opposite wall varied sinusoidally. The incompressible Navier–Stokes equations with Boussinesq approximation was solved by the SIMPLER algorithm. The heat transfer dependency on oscillation frequency was studied for different inclination angles.

Aktas et al. [32] numerically investigated thermal convection in a 2D resonator due to acoustic excitations induced by the vibration of the whole left sidewall. In their model, the left and right sidewalls were kept at the different temperature, while the top and the bottom walls were kept insulated. The mechanically induced periodic oscillations in the fluid were found to be insignificant on the heat transfer characteristics of the system (heated vertical wall), unless steady streaming flow were also present. In the present study, we consider a rectangular chamber with differentially heated top and bottom walls, while the left and right sidewalls are considered to be thermally insulated. In addition, the left sidewall vibrates with specified frequency and amplitude to excite standing waves in the chamber. Calculations are carried out with complete or partial left sidewall vibration. The developments of the flow, temperature and density fields induced by the vibrating left sidewall are predicted by directly solving the full compressible form of the Navier–Stokes equations. With this model, we are able to simulate the physical processes including the interaction of the wave field with viscous and thermal effects.

In the present paper, we focus on the enhancement of heat transfer by the acoustic streaming, and the behaviors of acoustic streaming under different wall temperature conditions. Unlike the past study [32], the acoustic wave propagation direction and the imposed temperature gradient in the enclosure are orthogonal and hence the effects of the acoustic perturbation on heat transfer is much more interesting. The characteristics of wave and temperature fields in the enclosure for the complete or partial wall vibrations are reported.

2. Problem geometry

A two-dimensional rectangular enclosures filled with nitrogen is considered (Fig. 1). The left wall of the enclosure vibrates harmonically, either completely or partially. The vibrating wall boundary condition is thus the acoustic energy source in this geometry. The displacement of vibration is given as $x = X_{\max}\sin(\omega t)$, where $\omega = 2\pi f$ is the angular frequency. The length of the enclosure is chosen as $L = 2x_0 = 8.825$ mm for all cases studied. The width of the enclosure (H) is varied in the cases studied. The frequency of the wall vibration is set as $f = 20$ kHz, and the corresponding wavelength of the sound waves is $\lambda = 17.65$ mm based on the undisturbed enclosure temperature $T_0 = 300$ K and pressure $P_0 = 1$ atm. Hence for the cases studied, $\lambda = 2L$.

One of the important parameters in the resonator is the viscous penetration depth $\delta_v = (2\nu/2\pi f)^{1/2} = 0.016$ mm. Here f is the frequency of the wall vibration and ν is the kinematic viscosity of the fluid. Previous studies already showed that the ratio of the resonator width H over δ_v play an important role in the acoustic-fluid dynamic interactions. In the present study, the resonator widths are limited to the range: H ($=2y_0$): $30\delta_v$–$50\delta_v$ (Table 1). In this width range, the behavior of acoustic streaming is most significant.

In the present study, the aspect ratio of the resonators L/H varied from 11.0 to 18.0. The width of the resonator was kept small such that the viscous penetration depth δ_v is well resolved in the simulations. To investigate the interaction between acoustic waves (propagating primarily in the x-direction) and heat transfer (in the y-direction), the top and bottom walls are set at different temperatures. As mentioned earlier, the vibrating left sidewall and the right sidewalls are thermally insulated.

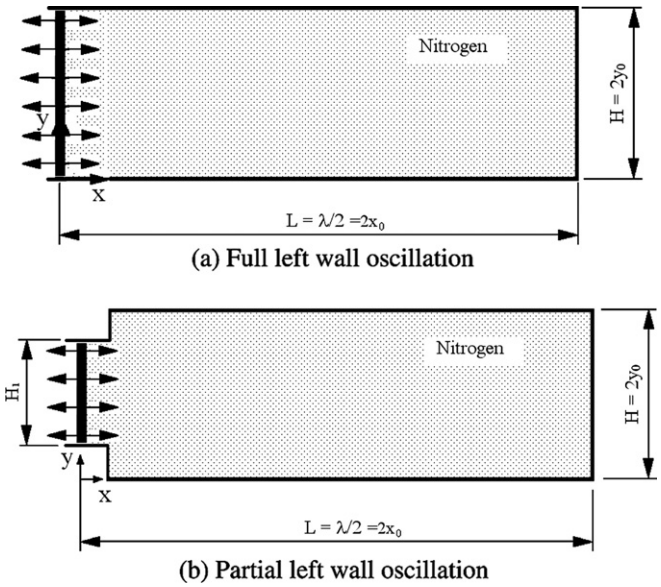

Fig. 1. Schematic of the computational domain.

Table 1
List of cases studied

No.	y_0/δ_v	x_0/δ_v	X_{max} (m)	H_1/H	ΔT (K)
1A	20	279	1.0×10^{-5}	1.0	0
1B					20
1C					60
2	20		0.5×10^{-5}	1.0	20
3	20		1.5×10^{-5}	1.0	20
4	15		1.0×10^{-5}	1.0	20
5	25		1.0×10^{-5}	1.0	20
6A	20		1.0×10^{-5}	0.4	0
6B					20
7	20		1.0×10^{-5}	0.1	0

3. Mathematical model

Thermal convection in acoustic streaming flow fields is described by the full Navier–Stokes and energy equations for a compressible fluid. In two-dimensional Cartesian coordinate system these equations are expressed as

$$\frac{\partial \rho}{\partial t} + \frac{\partial(\rho u)}{\partial x} + \frac{\partial(\rho v)}{\partial y} = 0 \tag{1}$$

$$\rho\frac{\partial u}{\partial t} + \rho u\frac{\partial u}{\partial x} + \rho v\frac{\partial u}{\partial y} = -\frac{\partial p}{\partial x} + \frac{\partial \tau_{xx}}{\partial x} + \frac{\partial \tau_{xy}}{\partial y} \tag{2}$$

$$\rho\frac{\partial v}{\partial t} + \rho u\frac{\partial v}{\partial x} + \rho v\frac{\partial v}{\partial y} = -\frac{\partial p}{\partial y} + \frac{\partial \tau_{yy}}{\partial y} + \frac{\partial \tau_{xy}}{\partial x} \tag{3}$$

$$\frac{\partial E}{\partial t} + \frac{\partial}{\partial x}[(E+p)u] + \frac{\partial}{\partial y}[(E+p)v] = \frac{\partial}{\partial x}[u\tau_{xx} + v\tau_{xy}] + \frac{\partial}{\partial y}[u\tau_{xy} + v\tau_{yy}] - \frac{\partial q_x}{\partial x} - \frac{\partial q_y}{\partial y} \tag{4}$$

Here t is time, x and y refer to the Cartesian coordinates, ρ is density, p is pressure, u and v are the velocity components, and E ($=\rho e$) is the total energy given by

$$E = \rho c_v T + \frac{1}{2}\rho(u^2+v^2) = \frac{p}{\gamma} + \frac{1}{2}\rho(u^2+v^2) \tag{5}$$

where γ is the ratio c_p/c_v.

The components of the stress tensor τ are

$$\tau_{xx} = \frac{4}{3}\mu\frac{\partial u}{\partial x} - \frac{2}{3}\mu\frac{\partial v}{\partial y}, \quad \tau_{yy} = \frac{4}{3}\mu\frac{\partial v}{\partial y} - \frac{2}{3}\mu\frac{\partial u}{\partial x}, \quad \tau_{xy} = \mu\left(\frac{\partial u}{\partial y} + \frac{\partial v}{\partial x}\right) \tag{6}$$

where μ is the dynamic viscosity. The components of the heat-flux vector are written as

$$q_x = -k\frac{\partial T}{\partial x}, \quad q_y = -k\frac{\partial T}{\partial y} \tag{7}$$

where k is the thermal conductivity and T is temperature. The temperature dependence of the viscosity and thermal conductivity are taken into account using the following expressions:

$$\mu = 0.3577 \times 10^{-6} T^{0.6885} \tag{8}$$

$$k = 0.3609 \times 10^{-3} T^{0.7512} \tag{9}$$

The gravitational effects on the flow fields are neglected in this study as the effects are considered to be negligible when compared to the flow fields produced by the vibration of the left wall. The temperature is related to the density and pressure through the ideal-gas law:

$$p = \rho R T \tag{10}$$

where R is the specific gas constant of the medium.

4. Numerical scheme

The governing equations (except the diffusion terms) are discretized using a control-volume-based flux-corrected transport (FCT) algorithm. FCT is a high order, nonlinear, monotone, conservative and positivity-preserving scheme designed to solve a general one-dimensional continuity equation with appropriate source terms [33]. This scheme has fourth-order accuracy in space and second order in time, which is able to resolve steep gradients with minimum numerical diffusion. Time-step splitting technique is used to solve the two-dimensional problem addressed here. Further details of the FCT algorithm used here are documented by Boris et al. [34]. The diffusion terms (the viscous term in the momentum equations and the conduction and viscous dissipation terms in the energy equation) were discretized using the central-difference approach and the time-step splitting technique was used to include the terms in the numerical scheme.

No-slip boundary conditions are used for all solid walls. A high-order non-dissipative algorithm such as FCT requires rigorous formulation of the boundary conditions. Otherwise, numerical solutions may show spurious wave reflections at the regions close to boundaries and nonphysical oscillations arising from instabilities. In the present computational method, the treatment proposed by Poinsot and Lele [35] is followed for implementing the boundary conditions for the density. This method avoids incorrect extrapolations and overspecified boundary conditions. Along any stationary solid wall, the density is calculated from

$$\left(\frac{\partial \rho}{\partial t}\right)_M + \frac{1}{c_M}\left(\frac{\partial p}{\partial n} + \rho c\frac{\partial u_n}{\partial n}\right)_M = 0 \tag{11}$$

where c is the acoustic speed, the subscript M indicates the location of the wall and n is the direction normal to the wall. Since the current problem involves a moving boundary and a time dependent boundary velocity, a modification in this part of the scheme is required for the left boundary. Along the vibrating wall, the density is calculated from

$$\frac{\partial \rho}{\partial t} = \frac{\rho\gamma}{c_L}\frac{\partial u_W}{\partial t} + \frac{\rho\gamma(u_W - c_L)}{c_L}\frac{\partial u}{\partial x} - \frac{\gamma(u_W - c_L)}{c_L^2}\frac{\partial p}{\partial x} \tag{12}$$

where c_L is the acoustic speed at the left wall. The acoustic speed c can be approximated as $\sqrt{\gamma RT}$. It is, however,

noted that from the present mathematical formulation, the acoustic speed can be directly obtained from the solution of the pressure field.

Typically a grid size of 150×98 is used for the rectangular domain. To accurately simulate the formation of acoustic streaming structures and heat transfer along the walls, resolving the boundary layer is essential. For this reason, we employ a non-uniform grid structure. This structure has finest grids in the vicinity of the walls and the grid quality gradually decreases as the distance from the horizontal walls increases. For the present calculations, there are always 3–5 grids inside the boundary layer. To model the wall vibration, moving cell boundaries [34] were considered for a few cells next to the left wall. The number of moving cell is chosen such that the maximum variation of a cell size is less than 25%.

5. Results and discussion

5.1. Validation results

To verify the numerical model and grid independency, the numerical model is first used to simulate a system similar to the one considered by Hamilton et al. [9] under the following conditions: $Pr = 0.67$, $\gamma = 5/3$, $y_0 = 20\delta_v$. The predicted steady streaming flow field (at the end of the 120th cycle) obtained by the present numerical method (where $f = 20$ kHz) is shown in Fig. 2. This cycle-averaged flow field is based on the average mass transport velocity values in the enclosure. The average mass transport (streaming) velocity is given by

$$U_{st} = \frac{\langle \rho u \rangle}{\langle \rho \rangle}, \quad V_{st} = \frac{\langle \rho v \rangle}{\langle \rho \rangle} \tag{13}$$

Here $\langle\ \rangle$ indicates the cycle-averaged quantities. The predicted streaming pattern and size are similar to those given by Hamilton et al. (not shown here), except that for the present calculations, the left and right vortices are not symmetric along the middle vertical-plane of the resonator. In the present case only the left wall vibrates, however, for the results given in Hamilton et al. the entire resonator vibrates, albeit with the same frequency and amplitude considered in the present simulations. Fig. 3(a) shows the comparison of the variation of the x-component of the cycle-averaged velocity along the enclosure height at $x/(L/2) = x/x_0 = 1.5$ from the present model predictions with the results given by Hamilton et al. Fig. 3(b) gives similar comparisons for the variation of the y-component of the cycle-averaged velocity along the enclosure height at $x/(L/2) = x/x_0 = 1.0$. In these two figures, the cycle-averaged velocities are nondimensionalized by $U_R = \frac{3}{16}\frac{U_{max}^2}{c}$, which is Rayleigh's result for the maximum streaming velocity in the center of a channel containing a viscous fluid. The maximum deviation that is found in Fig. 3 is 6%, which can be perhaps explained by the non-symmetric streaming structure due to the different wall conditions in the two studies.

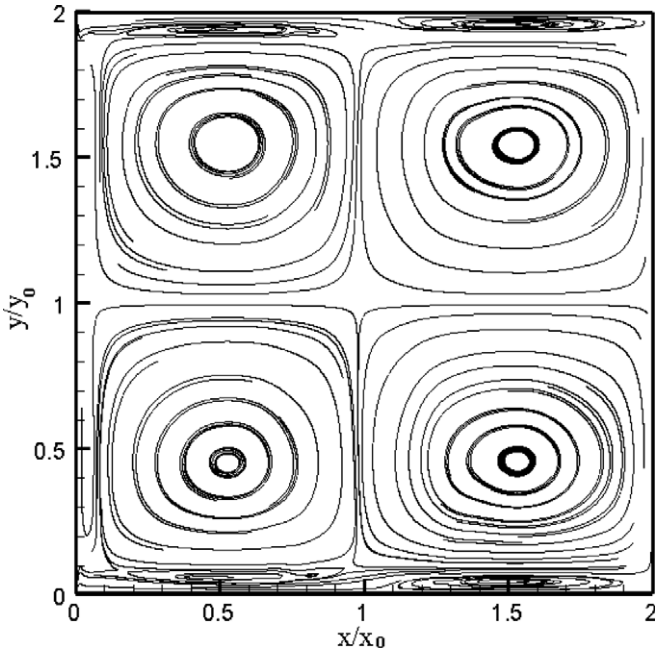

Fig. 2. End wall oscillation induced acoustic streaming (cycle-averaged values for the 120th cycle) for conditions given by Hamilton et al. [36].

5.2. Parametric case studies

After the verification of the mathematical formulation and the solution procedure, we investigate the effects of transverse acoustic waves on the convective heat transfer in the enclosure with imposed longitudinal temperature difference. Table 1 lists the cases reported in this paper. For each case, the calculations were started by keeping the top and bottom walls at the same temperatures. After the system achieves steady state, the top wall temperature is changed to investigate the interaction between heat transfer and acoustically driven flows.

In the first case considered (Case 1A), the maximum displacement of the left wall vibration is set to $x = X_{max}\sin(\omega t)$ with $X_{max} = 10$ μm, and $f = \omega/2\pi = f = 20$ kHz. The width of channel is set to $y_0 = 20\delta_v$. The temperature of the top and bottom walls are kept at the initial temperature $T_0 = 300$ K. The cycle-averaged steady state flow condition is achieved at about the 120th acoustic cycle.

Fig. 4(a) shows the pressure distribution along the horizontal mid-plane of the enclosure at $\omega t = 0$, $\pi/2$, π, $3\pi/2$ (during cycle # 120) for Case 1A. These pressure profiles remain essentially the same at any other horizontal plane away from the bottom and top walls and this indicates the near-one-dimensional character of the acoustic field in the bulk medium. The pressure distribution for $\omega t = 2\pi$ (not shown in Fig. 4) is identical to the curve given for $\omega t = 0$. At $\omega t = 0$ and $\omega t = \pi$, the amplitude of the pressure waves reach a maximum and a minimum value at the ends of the enclosure. At the beginning of the cycle ($\omega t = 0$), the pressure is maximum on the vibrating (left) wall of the enclosure and decreases with increasing distance from the wall and reaches a minimum value at $x \cong L$. The

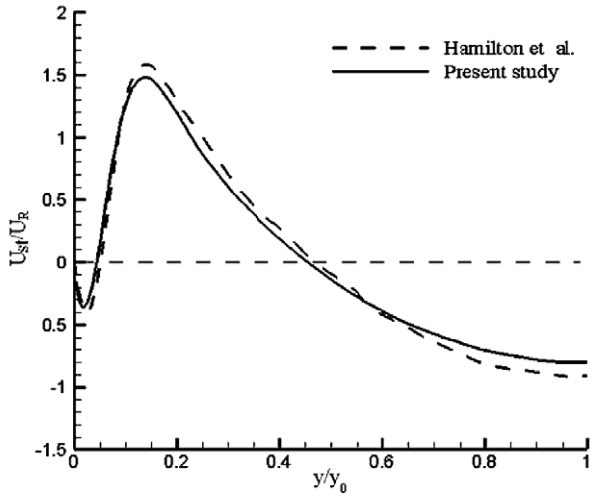

(a) x-component streaming velocity at $x/x_0 = 1.5$

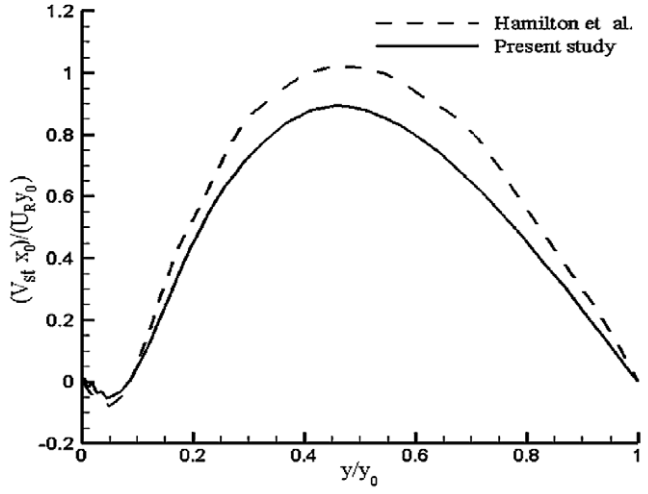

(b) y-component streaming velocity at $x/x_0 = 1.0$

Fig. 3. Comparison of the transverse distribution of streaming velocity with the results by Hamilton et al. [36].

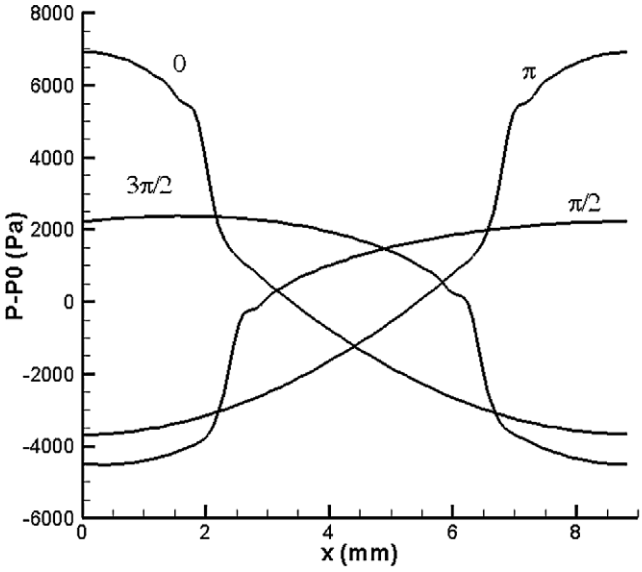

(a) Pressure

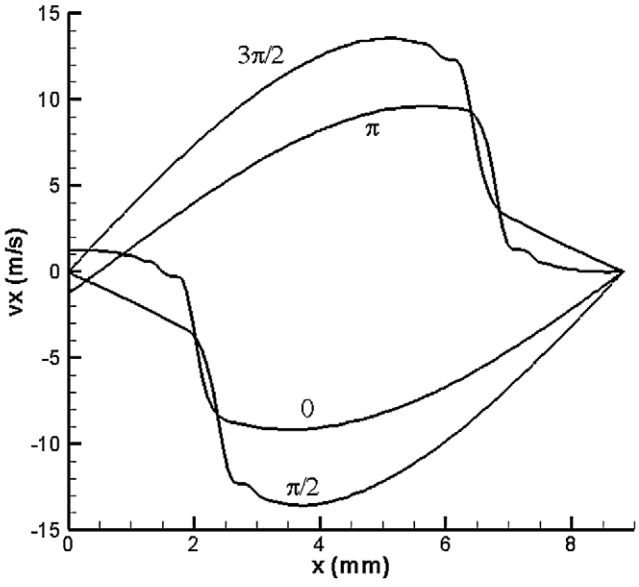

(b) x-component velocity

Fig. 4. Variations of pressure and the x-component of velocity along the horizontal mid-plane of the enclosure at four different instants ($\omega t = 0$, $\pi/2$, π, $3\pi/2$) in 120th cycle, isothermal top and bottom walls, $y_0/\delta_v = 20$, $X_{max} = 1.0 \times 10^{-5}$ (Case 1A).

behavior is quite opposite at $\omega t = \pi$ where the pressure is minimum on the vibrating (left) wall of the enclosure and increases with increasing distance from the wall and reaches a maximum value at $x \cong L$. The instantaneous u velocity profiles given in Fig. 4(b) for $\omega t = 0$, $\pi/2$, π and $3\pi/2$, along the horizontal mid-plane show that the velocity node is formed at approximately $x = L/2$. Cycle-averaged (120th cycle) solutions from the present simulations predict steady streaming flows in the enclosure. The predicted steady streaming flow field is shown in Fig. 5. At this stage, the predicted cycle-averaged velocity fields were found to be cycle-independent.

After the steady state is achieved (120th cycle), the top wall temperature is then increased to 320 K ($\Delta T = 20$ K), while the bottom wall is still kept at the initial temperature (Case 1B). Fig. 6 shows that cycle-averaged velocity field (121st cycle) changes drastically immediately after the heating is initiated. The steady streaming structure is destroyed due to the temperature change of the top wall. The gas flows from top to bottom, as heating of the top wall increases the local pressure in the upper part. The flow field is found to attain steady-state conditions again (in a cycle-averaged sense) by the 360th cycle. The new steady streaming flow field at the 360th cycle is shown in Fig. 7, where only two vortices (instead of the four shown in Fig. 5 earlier) are found. Thus the temperature difference between the top and the bottom walls affect the acoustically driven flow field in a significant way. Since the density, viscosity and conductivity values of the gas are temperature dependent, the symmetric streaming structure in Fig. 5 is

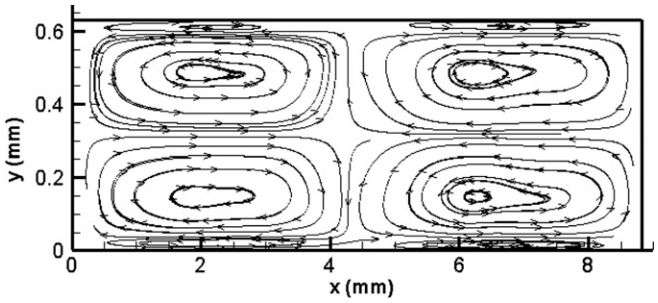

Fig. 5. Cycle-averaged flow field showing acoustic streaming at the 120th cycle, isothermal top and bottom walls, $y_0/\delta_v = 20$, $X_{max} = 1.0 \times 10^{-5}$ (Case 1A).

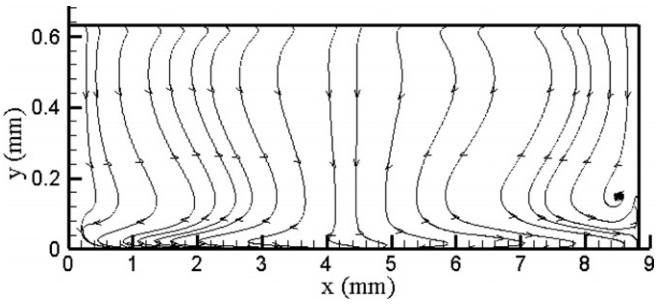

Fig. 6. Streamlines (cycle-averaged) immediately after differential heating along the top and the bottom walls, at 121st cycle, $y_0/\delta_v = 20$, $X_{max} = 1.0 \times 10^{-5}$ (Case 1B).

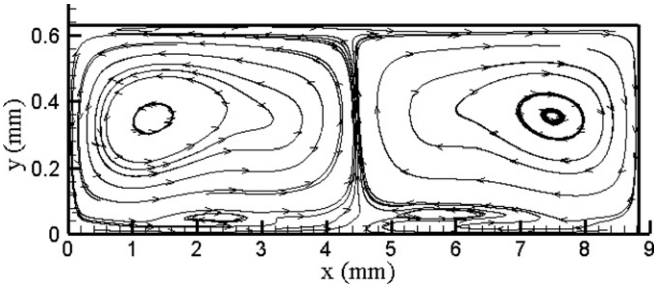

Fig. 7. Acoustic streaming in 360th cycle, differentially heated top and bottom wall, $y_0/\delta_v = 20$, $X_{max} = 1.0 \times 10^{-5}$ (Case 1B).

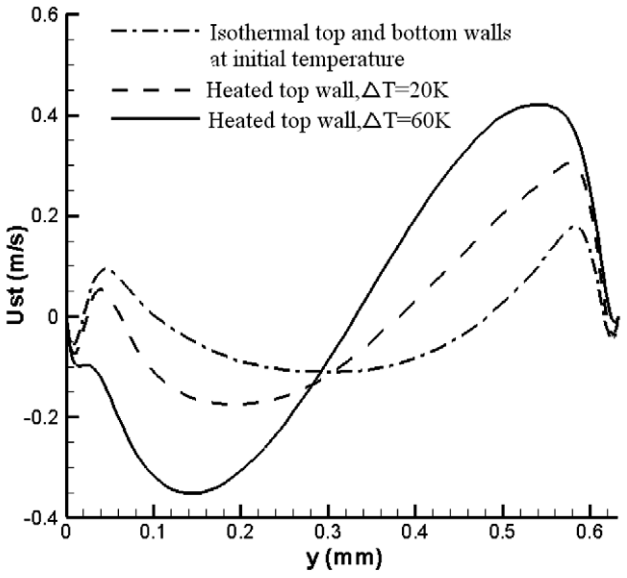

(a) x-component streaming velocity at x=3L/4

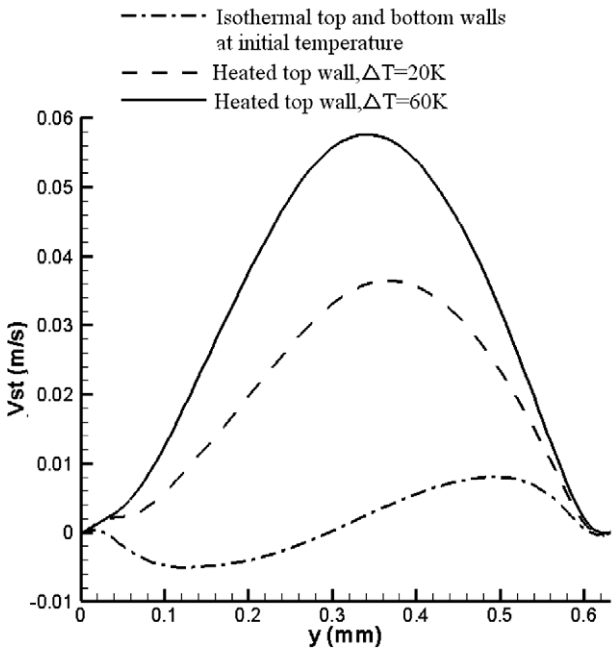

(b) y-component streaming velocity at x = L/2

Fig. 8. Variations of streaming velocity along the vertical-plane for different heating conditions along the top and bottom walls (Cases 1A, 1B and 1C).

distorted and we essentially have a rather asymmetric (cycle-averaged) flow field.

To further study the effect of temperature difference on streaming velocity, we increase the top wall temperature to 360 K from 320 K (Case 1C). For the three different heating cases (1A, 1B and 1C), x-component of the cycle-averaged streaming velocity profiles along the vertical-plane at $x = 3L/4$ are given in Fig. 8(a), and the y-component of the cycle-averaged streaming velocity profiles along the vertical-plane at $x = L/2$ are shown in Fig. 8(b). Compared with the unheated case (1A), velocity profiles change dramatically due to the streaming structure changes for Cases 1B and 1C. The streaming velocity components also increase when the top wall temperature increase. Consequently, differential heating increases the strength of acoustic streaming, though the symmetrical structure found in Fig. 5 (Case 1A) is destroyed.

The cycle-averaged temperature contours are shown in Fig. 9 for $T_{top} = 320$ K (Case 1B). The effect of the cycle-averaged flow field (Fig. 7) on the temperature field is evident. The variation of cycle-average temperature along the vertical plane of the enclosure at three different locations ($x = L/4$, $L/2$, $3L/4$) are given in Fig. 10 (Case 1B) along with the conduction profile (no acoustic perturbation). The maximum heat transfer to the horizontal walls is found

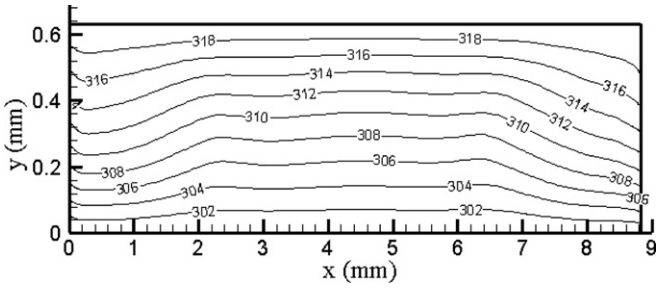

Fig. 9. Cycle-average temperature contours, at the 360th cycle, differentially heated top and bottom walls, $y_0/\delta_v = 20$, $X_{max} = 1.0 \times 10^{-5}$ (Case 1B).

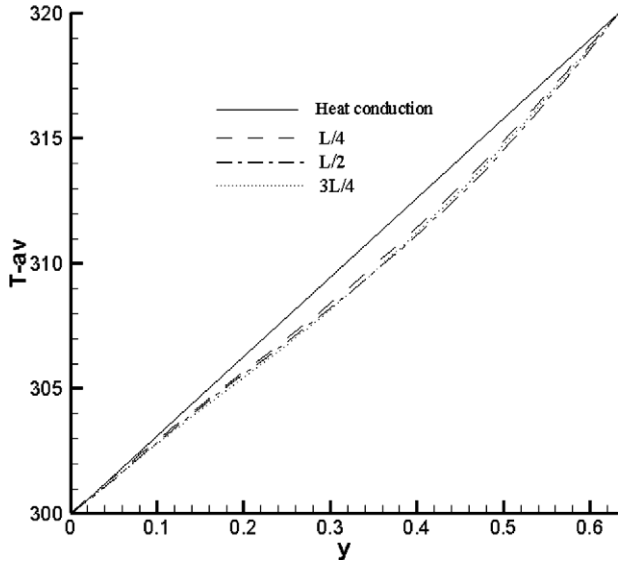

Fig. 10. Variation of cycle-averaged temperature along the vertical plane of the enclosure at three different locations ($x = L/4$, $L/2$, $3L/4$), at the 360th cycle, differentially heated top and bottom walls, $y_0/\delta_v = 20$, $X_{max} = 1.0 \times 10^{-5}$ (Case 1B).

at the middle of resonator, where the mean streaming flow is strongest. The spatially and cycle-averaged Nusselt number, $\overline{Nu}$ along the top and bottom walls are found to be 0.998 and 1.231, respectively. The asymmetry is due to the acoustic power input from the left wall vibration. The acoustic power input to the system is converted to thermal energy by the viscous dissipation (see Eq. (4)), which increases the bottom wall heat load, compared to the top wall.

To further study the effects of wall vibration amplitude on the heat transfer, simulations are run for different amplitudes: $X_{max} = 0.5 \times 10^{-5}$ m (Case 2) and $X_{max} = 1.5 \times 10^{-5}$ m (Case 3) with $\Delta T = 20$ K. For the different wall vibration amplitudes, there is no significant difference on the streaming structure compared to the results obtained for Case 1B ($X_{max} = 1.0 \times 10^{-5}$ m). The corresponding cycle-averaged (360th cycle) temperature contours are shown in Fig. 11(a) and (b). For lower acoustic power input (Case 2), the isotherms are similar to those obtained for the heat conduction case. For higher acoustic

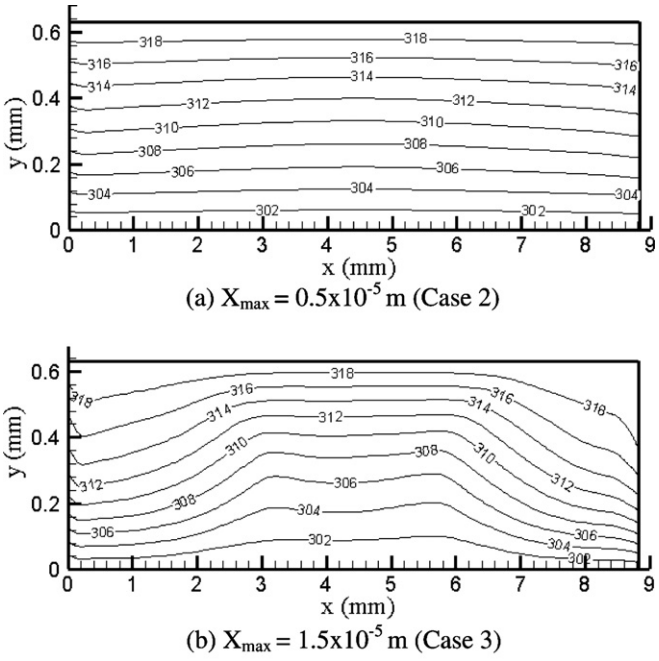

Fig. 11. Cycle-average temperature contours in 360th cycle for different X_{max}, differentially heated top and bottom walls, $y_0/\delta_v = 20$, Cases 2 and 3.

power input (Case 3) compared to Case 1B, the temperature field undergoes further distortion to accommodate the larger acoustic power input.

Cases 4 and 5 are run for different channel widths $y_0 = 15\delta_v$, and $25\delta_v$, respectively, with $\Delta T = 20$ K. In this

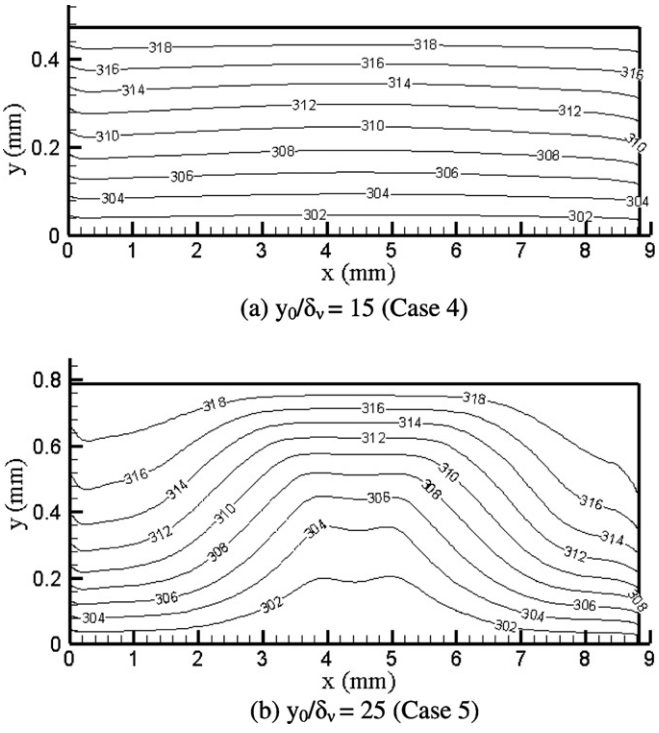

Fig. 12. Cycle-average temperature contour in 360th cycle for different widths, differentially heated top and bottom walls, $X_{max} = 1.0 \times 10^{-5}$, Cases 4 and 5.

range, the predicted streaming structures do not change much compared to results obtained for Case 1B ($y_0 = 20\delta_v$). However, the temperature contours for $y_0 = 15\delta_v$ (Fig. 12(a)) and $y_0 = 25\delta_v$ (Fig. 12(b)) show significant differences. For a larger enclosure height, the acoustic power input is higher and the temperature field shows more distortion. The effect of enclosure height on mean $\overline{Nu}$ is given in the Table 2. $\overline{Nu}$ along the bottom wall increases significantly with the increasing channel width, but the Nu along top wall does not change much. To compensate for the energy addition by the vibrating wall, the heat addition from the hot wall to the fluid is lesser than the heat removal from the bottom wall.

Next we consider a more realistic system where the vibration of the left wall is limited to the central region of the wall, H_1. We consider the vibration of part of left wall: $H_1/H = 0.4$ (Case 6), and 0.2 (Case 7), see Fig. 1(b).

Table 2
Effect of enclosure width on Nu

Case	y_0/δ_v	Top wall	Bottom wall
1B	20	0.998	1.231
4	15	1.016	1.114
5	25	1.098	1.395

Fig. 13(a) shows the cycle-averaged flow field (360th cycle) for Case 6, where 40% of the left wall vibrates, under unheated (isothermal top and bottom walls) condition. In the bulk zone, four outer streaming and four inner streaming rolls are observed, similar to the case of the full wall vibration (see Fig. 5). However, two other additional vortices are found near the central vibrating part of the left wall. The steaming patterns near the left wall are enlarged in the Fig. 13(b), which clearly shows the effects of the partial vibration on the flow field.

Following earlier simulations with full wall vibration (Cases 1A and 1B), the top wall temperature is now increased to 320 K, while the bottom wall is held at 300 K (Case 6B). The cycle-averaged flow field (after an additional 360 cycles) is given in Fig. 14. The results are similar to those reported earlier in Fig. 7 (for the full wall vibration). The effect of the partial wall vibration is only limited to the vicinity to the left wall. Fig. 15 shows the cycle-averaged (360th cycle) temperature contours for Case 6B. It is close to the results of heat conduction, because of the weak streaming velocity.

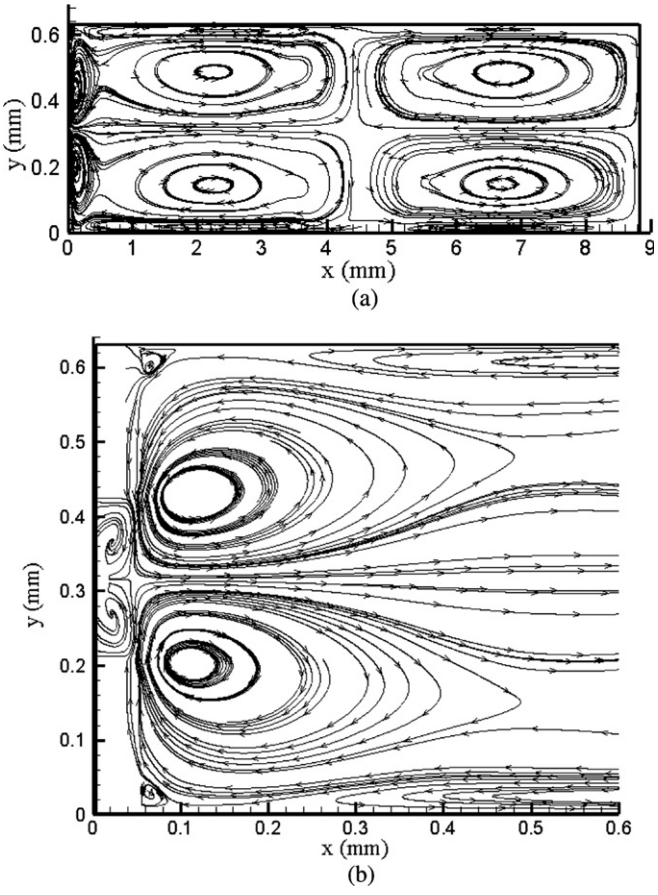

Fig. 13. Acoustic streaming, at 120th cycle, isothermal top and bottom walls, $y_0/\delta_v = 20$, $X_{max} = 1.0 \times 10^{-5}$, partial (40%) left wall vibration, (Case 6A).

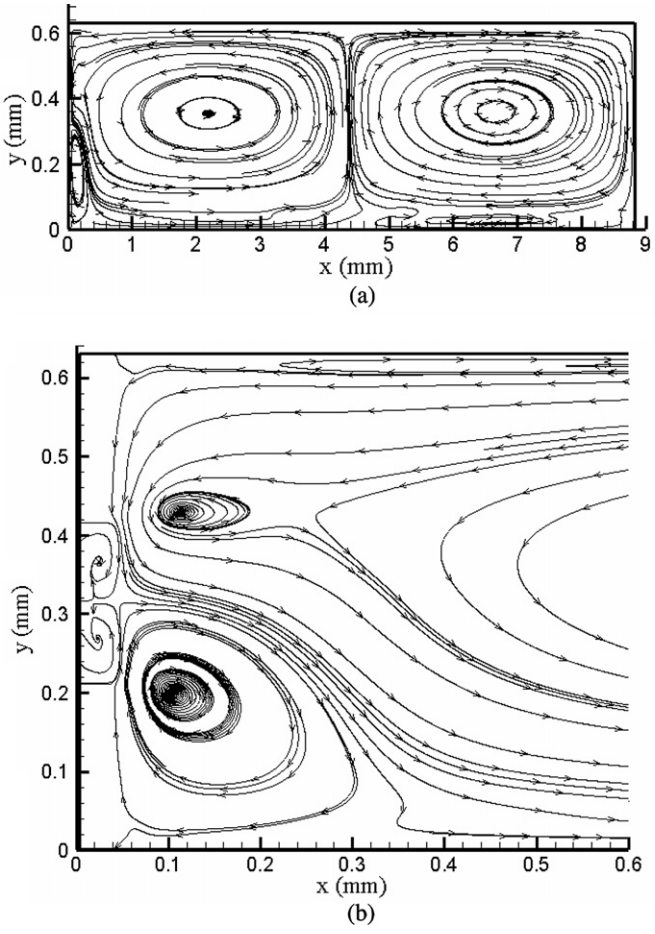

Fig. 14. Acoustic streaming, at 360th cycle, $y_0/\delta_v = 20$, $X_{max} = 1.0 \times 10^{-5}$, differentially heated top and bottom wall, partial (40%) left wall vibration, (Case 6B).

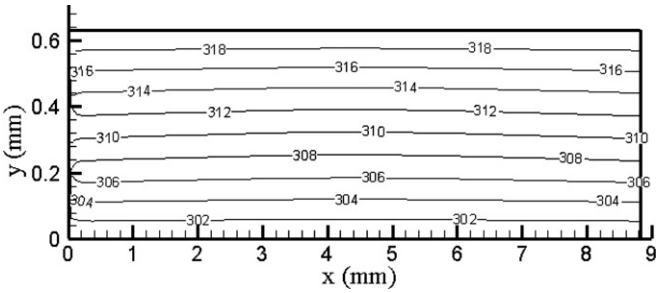

Fig. 15. Cycle-average temperature contour, in 360th cycle, differentially heated top and bottom wall, $y_0/\delta_v = 20$, $X_{max} = 1.0 \times 10^{-5}$, 40% of left wall vibrates, (Case 6B).

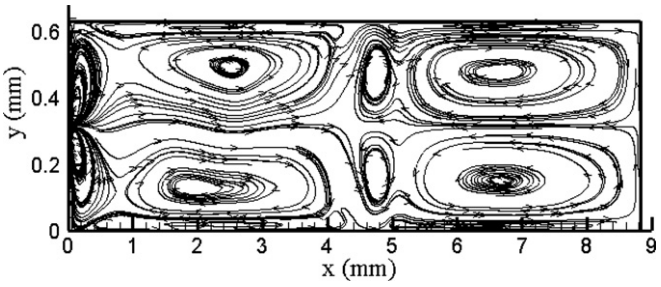

Fig. 16. Acoustic streaming, in 120th cycle, isothermal top and bottom walls, $y_0/\delta_v = 20$, $X_{max} = 1.0 \times 10^{-5}$, partial (10%) left wall vibration, (Case 7).

In Case 7, the vibrating part of the left wall is further deceased to 10%. The acoustic streaming when the top and bottom walls are kept at the initial temperature is shown in Fig. 16. The streaming structure becomes irregular, because of the nonuniform boundary condition in the left wall and weaker acoustic streaming in the field.

6. Conclusions

The convective flows in a nitrogen-filled differentially heated enclosure induced by a vibrating sidewall were investigated numerically. The high resolution calculations predict the development of acoustic streaming in the flow field. The structure and strength of the steady streaming structures generated by wall vibration are affected when an orthogonal temperature gradient exists in the enclosure due to differential heating of the top and the bottom walls. The formation of pressure (acoustic) waves and associated thermal and flows phenomena are predicted by solving the unsteady compressible Navier–Stokes equations with temperature dependent viscosity and conductivity. The governing equations are solved by utilizing a highly accurate flux corrected transport (FCT) algorithm. The steady second-order acoustic streaming is recovered from the temporal solutions by cycle-averaging the solutions. The streaming velocities are found to increase when the temperature of heated wall is increased, albeit at the cost of asymmetry in the flow field. The effect of partial wall vibration is also studied. Partial wall vibration is found to affect the solution only locally in the enclosure. The model developed can be a valuable tool in the optimized design of heat exchangers with acoustic perturbations.

References

[1] Lord Rayleigh, On the circulation of air observed in Kundt's tubes, Philos. Trans. A 175 (1884) 1–21.
[2] P.J. Westervelt, The theory of steady rotational flow generated by a sound field, J. Acoust. Soc. Am. 25 (1) (1953) 60–67.
[3] W.L. Nyborg, Acoustic streaming due to attenuated plane waves, J. Acoust. Soc. Am. 25 (1) (1953) 68–75.
[4] W.L. Nyborg, Acoustic streaming near a boundary, J. Acoust. Soc. Am. 30 (4) (1958) 329–339.
[5] Q. Qi, The effect of compressibility on acoustic streaming near a rigid boundary for a plane traveling wave, J. Acoust. Soc. Am. 94 (2) (1993) 1090–1098.
[6] Q. Qi, R.E. Johnson, J.G. Harris, Boundary layer attenuation and acoustic streaming accompanying plane-wave propagation in a tube, J. Acoust. Soc. Am. 97 (3) (1995) 1499–1509.
[7] P. Vainshtein, Rayleigh streaming at large Reynolds number and its effect on shear flow, J. Fluid Mech. 285 (1995) 249–264.
[8] M.F. Hamilton, Y.A. Ilinskii, E.A. Zabolotskaya, Acoustic streaming generated by standing waves in two-dimensional channels of arbitrary width, J. Acoust. Soc. Am. 113 (1) (2003) 153–160.
[9] M.F. Hamilton, Y.A. Ilinskii, E.A. Zabolotskaya, Thermal effects on acoustic streaming in standing waves, J. Acoust. Soc. Am. 114 (6) (2003) 3092–3101.
[10] P.D. Richardson, Heat transfer from a circular cylinder by acoustic streaming, J. Fluid Mech. 30 (2) (1967) 337–355.
[11] P.D. Richardson, Local effect of horizontal and vertical sound fields on natural convection from a horizontal cylinder, J. Sound Vib. 10 (1) (1969) 32–41.
[12] H. Engelbrecht, L. Pretorius, The effect of sound on natural convection from a vertical flat plate, J. Sound Vib. 158 (1) (1992) 213–218.
[13] A. Gopinath, A.F. Mills, Convective heat transfer from a sphere due to acoustic streaming, J. Heat Transfer 115 (1993) 332–341.
[14] A. Gopinath, A.F. Mills, Convective heat transfer due to acoustic streaming across the ends of a Kundt tube, J. Heat Transfer 116 (1994) 47–53.
[15] P. Vainshtein, M. Fichman, C. Gutfinger, Acoustic enhancement of heat transfer between two parallel plates, Int. J. Heat Mass Transfer 38 (10) (1995) 1893–1899.
[16] G. Mozurkewich, Heat transfer from a cylinder in an acoustic standing wave, J. Acoust. Soc. Am. 98 (4) (1995) 2209–2216.
[17] A. Gopinath, D.R. Harder, An experimental study of heat transfer from a cylinder in low-amplitude zero-mean oscillatory flows, Int. J. Heat Mass Transfer 43 (2000) 505–520.
[18] G. Mozurkewich, Heat transport by acoustic streaming within a cylindrical resonator, Appl. Acoust. 63 (2002) 713–735.
[19] T. Yano, Turbulent acoustic streaming excited by resonant gas oscillation with periodic shock waves in a closed tube, J. Acoust. Soc. Am. 106 (1) (1999) L7–L12.
[20] M.K. Aktas, B. Farouk, Numerical simulation of acoustic streaming generated by finite-amplitude resonant oscillation in an enclosure, J. Acoust. Soc. Am. 116 (5) (2004) 2822–2831.
[21] S. Boluriaan, P.J. Morris, Acoustic streaming: from Rayleigh to today, Int. J. Aeroacoust. 2 (2003) 255–292.
[22] M. Kawahashi, M. Arakawa, Nonlinear phenomena induced by finite-amplitude oscillation of air column in closed duct, JSME Int. J. 39 (2) (1996) 280–286.
[23] M. Kawahashi, M. Tanahashi, M. Arakawa, H. Hirahara, Visualization and measurement of acoustic streaming coupling with natural convection, ASME/JSME Fluids Engineering and Laser Anemometry Conference and Exhibition, Hilton Head, SC, USA, 1995.

[24] B. Loh, S. Hyun, P.I. Ro, C. Kleinstreuer, Acoustic streaming induced by ultrasonic flexural vibrations and associated enhancement of convective heat transfer, J. Acoust. Soc. Am. 111 (2) (2002) 875–883.
[25] B. Loh, D. Lee, Heat transfer characteristics of acoustic streaming by longitudinal ultrasonic vibration, J. Thermophys. Heat Transfer 18 (1) (2004) 94–99.
[26] Q. Wan, A.V. Kuznetsov, Numerical study of the efficiency of acoustic streaming for enhancing heat transfer between two parallel beams, Flow Turbul. Combust. 70 (2003) 89–114.
[27] Q. Wan, T. Wu, J. Chastain, W.L. Roberts, A.V. Kuznetsov, P.I. Ro, Forced convective cooling via acoustic streaming in a narrow channel established by a vibrating piezoelectric bimorph, Flow Turbul. Combust. 74 (2005) 195–206.
[28] Q. Wan, A.V. Kuznetsov, Investigation of hysteresis in acoustically driven channel flow at ultrasonic frequency, Numer. Heat Transfer Part A (2005) 137–146.
[29] Q. Wan, A.V. Kuznetsov, Streaming in a channel bounded by an ultrasonically oscillating beam and its cooling efficiency, Numer. Heat Transfer Part A (45) (2004) 21–47.
[30] C.-H. Cheng, K.-S. Hung, Numerical predictions of thermal convection in a rectangular enclosure with oscillating wall, Numer. Heat Transfer Part A 48 (2005) 791–809.
[31] E.V. Kalabin, M.V. Kanashina, P.T. Zubkov, Heat transfer from the cold wall of a square cavity to the hot one by oscillatory natural convection, Numer. Heat Transfer Part A 47 (2005) 609.
[32] M.K. Aktas, B. Farouk, Y. Lin, Heat transfer enhancement by acoustic streaming in an enclosure, J. Heat Transfer 127 (2005) 1313–1321.
[33] E.S. Oran, J.P. Boris, Numerical Simulation of Reactive Flows, Cambridge University Press, Cambridge, England, 2000.
[34] J.P. Boris, A.M. Landsberg, E.S. Oran, J.H. Gardner, LCPFCT- A Flux-Corrected Transport Algorithm for Solving Generalized Continuity Equations, Naval Research Laboratory, Washington, DC, 1993.
[35] T.J. Poinsot, S.K. Lele, Boundary conditions for direct simulations of compressible viscous flows, J. Comput. Phys. 101 (1992) 104–129.
[36] C. Borgnakke, P.S. Larsen, J. Comp. Phys. 18 (1975) 405.